Decoding the spherical harmonics for 3D medical image processing and retrieval

LEILA CRISTINA C. BERGAMASCO*, Graduate Program in Electrical Engineering, Escola Politécnica da Universidade de São Paulo, Brazil
FÁTIMA L. S. NUNES†, Laboratory of Computer Applications for Healthcare, School of Arts, Sciences and Humanities, Engineering School - Universidade de São Paulo, Brazil

Spherical harmonics (SPHARMs) have been widely used in many areas of Computer Graphics to solve problems of three-dimensional (3D) modeling. Due to considerable dissemination of 3D objects in everyday life, the SPHARMs concept has also been extended to shape analysis and classification proposals. However, despite an important theory behind SPHARM, few articles adequately explain its operation and its proper applicability in real problems. Thus, this article aims to: 1) demystify the SPHARMs concept and development through a tutorial concerning their end-to-end implementation; and 2) provide visibility of its use, through experiments with both a controlled set of synthetic 3D objects and a left ventricle set reconstructed from Resonance Magnetic images. We obtained 100% of accuracy for synthetic 3D objects and 85.6% for 3D medical objects. In addition, our algorithm has a computational efficiency of $O(n^2)$ for both scenarios, supporting the robustness of SPHARMs for 3D objects processing and shape analysis.

CCS Concepts: • **Information systems** → **Image search**; • **Applied computing** → **Physics**; **Health informatics**; • **Computing methodologies** → *Shape analysis*.

Additional Key Words and Phrases: Spherical harmonics, medical images, feature extraction, coefficient decomposition, left ventricle

ACM Reference Format:
Leila Cristina C. Bergamasco and Fátima L. S. Nunes. 2020. Decoding the spherical harmonics for 3D medical image processing and retrieval. *ACM Comput. Surv.* 1, 1 (March 2020), 22 pages. https://doi.org/0000001.0000001

1 INTRODUCTION

One of the first references to Spherical Harmonics (SPHARMs) dates to the 1860s, in the *Treatise on Natural Philosophy* [46]. In this work, SPHARMs are described as homogeneous functions which satisfy Laplace's equation (Eq.(1)) using spherical coordinates.

$$\frac{\partial^2 f}{\partial x^2} + \frac{\partial^2 f}{\partial y^2} + \frac{\partial^2 f}{\partial z^2} = 0 \tag{1}$$

*PhD
†PhD, Full Professor and Head of the Information Technology Center of University of Sao Paulo

Authors' addresses: Leila Cristina C. Bergamasco, Graduate Program in Electrical Engineering, Escola Politécnica da Universidade de São Paulo, Av. Prof. Luciano Gualberto, travessa 3, 380, Sao Paulo, Sao Paulo, 05508-010, Brazil, leila.cristina@usp.br; Fátima L. S. Nunes, Laboratory of Computer Applications for Healthcare, School of Arts, Sciences and Humanities, Engineering School - Universidade de São Paulo, Av. Arlindo Béttio, 1000, Sao Paulo, Sao Paulo, 03828-000, Brazil, fatima.nunes@usp.br.

0360-0300/2020/3-ART $15.00
https://doi.org/0000001.0000001

The SPHARMs have been used in several knowledge domains such as quantum mechanics, electromagnetism, molecular representation, and geophysics [4, 52]. In the area of Computer Science, SPHARMs are an important concept mostly applied in graphics to solve problems related to three-dimensional (3D) shape modeling, representation and light. Additionally, they can be used for 3D shape representation and, consequently, for 3D objects retrieval.

These several option for SPHARMs utilization come from their orthogonality property. Each SPHARM is orthogonal to each other, which allows expanding the Fourier series in an infinite set of SPHARMs [1]. In practical terms, this means that it is possible to use the Fourier coefficients for modeling, reconstructing, and as shape feature descriptor of 3D objects [49]. Additionally, some authors have pointed out additional advantages related to implementing SPHARMs, such as the low computational cost [53] and the and the invariance to scale, rotation, and translation [26, 53].

However, the SPHARMs theory and development is not trivial. Although some papers have presented the SPHARMs concept [5, 11, 12, 21], none of them have fully explained their development process. Some authors mention software to perform their calculations, but they omit chosen parameters [11, 43, 52]. These aspects make it difficult to reproduce the experiments.

Given the relevance of SPHARMs and a lack of explanations about their theory and implementation in the literature, this tutorial-based paper provides a end-to-end explanation about SPHARMs, which is unprecedented in current SPHARMs literature. We also performed experiments using two sets of 3D objects to demonstrate, test and validate our tutorial: the first set is composed of synthetic 3D structures and the second is composed of 3D medical objects of left ventricles, whose surfaces were reconstructed from Magnetic Resonance Imaging (MRI) slices.

This article is organized as follows: Section 2 presents an overview about current scenarios where the SPHARMs are applied; Section 3 explains the SPHARMs theory and development; Section 4 describes the experiments and materials; Section 5 shows the experiments results; Section 6 discusses the results found, and Section 7 presents the final remarks.

2 BACKGROUND

We conducted an exploratory analysis about SPHARMS and we analyzed 30 papers, Fig. 1 shows the results according the objective of the papers. and identified four main goals on the utilization of SPHARMs: 3D objects Reconstruction and Modeling (37%), Shape analysis (37%), Segmentation (16%), and Classification (10%).

The shape analysis was largely used in studies to analyze and compare 3D medical objects shape, e.g., volume or boundary with a ground truth [2, 42, 43]. Some articles within the reconstruction scope also compare 3D surfaces with a ground truth, but the main goal of these papers was to improve the reconstruction precision and efficiency [21, 23]. A common characteristic among all the selected papers was the utilization of SPHARM coefficients (a_{lm}) as the main data considered for comparison/reconstruction. Table 1 presents a brief description of the main aspects of the analyzed papers.

In our search we did not find papers about using SPHARMs to retrieve 3D medical objects, instead, we found articles about performing 3D retrieval in generic objects as chair, lamps, and cars [39, 50]. In the medical scenario, the most similar papers are those that perform shape analysis, from the features extracted using SPHARMs can be applied in the retrieval process.

The first paper to introduce this issue regarding 3D object retrieval with SPHARMs, belongs to Saupe and Vranic [39],who compared SPHARMs coefficients and Moment-Based in the retrieval task, considering 3D generic objects. According to the authors, the results showed that SPHARMs had better performance. Similarly, in [50] SPHARMs coefficients were applied to create multidimensional feature vectors and the nearest neighbors were used to rank 3D objects.

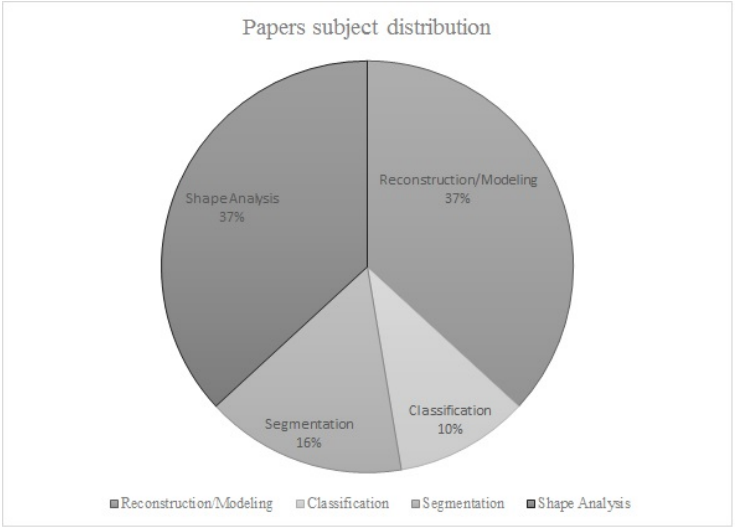

Fig. 1. Papers distribution according to their goals.

Table 1. Categorization of the articles using SPHARMs in the literature search.

Subject	Main goals	Papers related
Reconstruction and Modeling	Improve the reconstruction efficiency and precision, using few SPHARM coefficients but keeping the precision.	[21–23, 27, 29, 30, 45]
Classification	Based on SPHARMs coefficients, classify 3D anatomical structures according to its shape information.	[28, 32]
Segmentation	Authors used the SPHARMs coefficients to help other segmentation techniques such as orientation distribution functions to segment anatomical structures.	[5, 12, 48]
Shape analysis	With the SPHARM coefficients, the authors could estimate organ motion, wall thickness and volume.	[3, 10, 11, 13, 15, 17, 42, 43]

An important improvement on SPHARMs was made by Kazhdan et al.*et al.* [25], who turned SPHARMs coefficients invariant to rotation, increasing the SPHARMs potential to describe shape features. The authors used a set of 1890 3D “household" objects to test their approach.

As previously mentioned, some papers were intended to describe SPHARMs, such as Wang *et al.* [52], who provided a good description of SPHARMs coefficients computation; however, these researchers did not explain some important concepts such as the Legendre polynomials, the normalization factor and complex exponential computation. Additionally, it is unclear how they chose the number of coefficients. On the other hand, Morris *et al.* [35] conducted a useful analysis of SPHARMs theory, but they did not provide details about the implementation.

Other publications, such as technical notes [40], personal appointments [34], and papers focused on 3D diffused light [19, 41] also present SPHARMs, but none of them explain the whole computation process, which is one of the goals of the present article.

3 SPHERICAL HARMONICS DESCRIPTOR

SPHARMs are composed of a complete basis set of orthogonal functions. This characteristic is a consequence of the Sturm-Liouville form of the Laplace Equation.

This property means that any spherical function $f(\theta, \phi)$ can be expressed as a linear combination of its harmonics as on Eq.(2) [1]. The term a_{lm} complex coefficients matrix; these coefficients are the analogue to the three dimensional Fourier coefficients. The terms $Y_l^m(\theta, \phi)$ are SPHARMs of degree l and order m for the spherical coordinates (θ, ϕ).

$$f(\theta, \phi) = \sum_{l}^{\infty} \sum_{m=-l}^{l} a_{lm} Y_l^m(\theta, \phi) \tag{2}$$

Fig. 2 presents the SPHARMs computation schema. Each part of this schema will be detailed in the next sections.

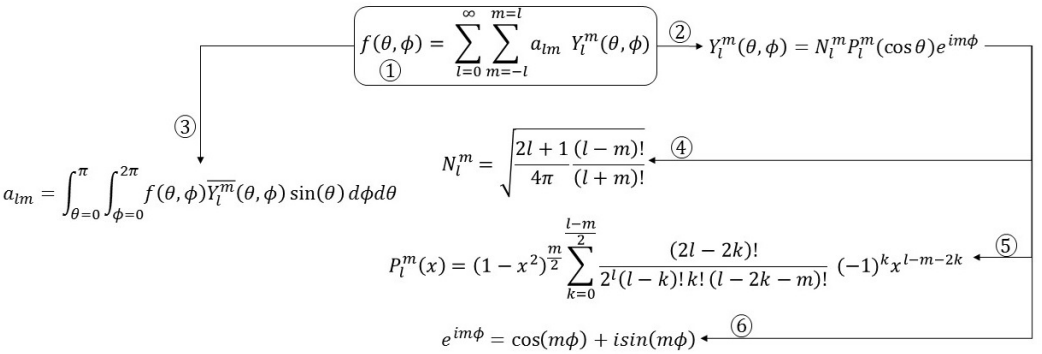

Fig. 2. SPHARMs computation (1) can be divided in two parts: harmonics computation (2) and coefficient matrix computation (3). Harmonics computation is subdivided in three parts: Normalization factor computation (4), Associated Legendre polynomials computation (5), and complex exponential computation (6).

3.1 Spherical harmonic $Y_l^m(\theta, \phi)$

The term $Y_l^m(\theta, \phi)$ is the harmonic for a specific degree l, order m and spherical coordinates (θ, ϕ). The spherical coordinate θ represents the polar angle, and ϕ represents the azimuth.

Here is the first important detail of SPHARMs: we based the present discussion on Physics theory where $\theta \in [0, \pi]$ and $\phi \in [0, 2\pi]$ [14]. However, in the works of several mathematicians, θ is used for azimuthal angle and ϕ is used as polar angle. Thus, attention is necessary for the equations used to calculate these parameters.

SPHARMs computation also considers the parameters l and m, where $l \in \mathbb{N}$ and $m \in [-l, l]$. These parameters represent the degree and the order of the SPHARMs and determine how much the spherical functions will expand. (this can impact, for example, the number of complex coefficients a_{lm} generated and how much details the 3D modeling will contain); 2) determine the nodal lines (longitudinal or latitudinal) of the unit sphere in the SPHARMs representation. To determine the longitudinal lines, the m value is used, and for latitudinal lines the absolute difference between l

and m is computed. Fig. 3 shows an example of a unit sphere with nodal lines for different values of l and m [40].

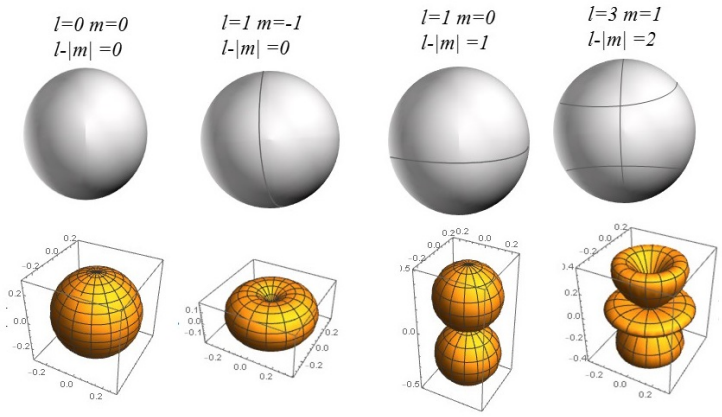

Fig. 3. Spherical harmonics representation using different values of l and m: the first line is the concept of nodal lines division and the second is the graphic appearance after plotted.

The Eq.(3) shows the $Y_l^m(\theta, \phi)$ computation, which is composed of three components: normalization factor, associated Legendre polynomials and complex exponential.

$$Y_l^m(\theta, \phi) = N_l^m P_l^m(cos\phi) e^{im\phi} \tag{3}$$

The normalization factor is a constant expressed by the explicit function presented in Eq.(4) [1].

$$N_l^m = \sqrt{\frac{2l+1}{4\pi} \frac{(l-m)!}{(l+m)!}} \tag{4}$$

Another important component of the SPHARMs computation is the Associated Legendre polynomials, which are solutions for the general Legendre equation [20]. These polynomials can be expressed using an explicit sum, where l and m are the same parameters of degree and order, and k changes according to the l and m values, having zero as initial value. This sum function arises from the Taylor series of Legendre polynomials.

$$P(x)_l^m = (1-x^2)^{\frac{m}{2}} \sum_{k=0}^{\frac{l-m}{2}} \frac{(2l-2k!)}{2^l (l-k)!k!(l-2k-m)!} H$$
$$H = (-1)^k x^{(l-2k-m)} \tag{5}$$

The last part of SPHARMs computation is the complex exponential. According to the SPHARMs theory, this calculation results in a complex number. We can use Euler's identity to compute this term. Eq.(6) presents the Euler's identity, where m is the SPHARM order, ϕ is the azimuth angle and i is the imaginary part of the complex number [1].

$$e^{im\phi} = cos(m\phi) + isin(m\phi) \tag{6}$$

3.1.1 $Y_l^m(\theta,\phi)$ particularities. The computation of $Y_l^m(\theta,\phi)$ has also some particularities which need to be taken into account. The first one is the phase factor $(-1)^m$, called Condon-Shortley phase [1], whose main objective is facilitate the angular momentum computation. This phase factor can be included in the Associated Legendre polynomials for negative m values (Eq.(7)) or at the end of Y_l^m computation, as in Eq.(8). It is important to highlight that in Eq.(8) the Condon-Shortley phase is used for both, positive and negative values of m.

$$P(x)_l^{-m} = (-1)^m \frac{(l-m)!}{(l+m)!} P(x)_l^m \tag{7}$$

$$Y_l^m(\theta,\phi) = (-1)^m N_l^m P_l^m e^{im\phi} \tag{8}$$

Additionally, for negative values of m it is necessary to calculate the complex conjugate of Y_l^m, as demonstrated in Eq.(9) by the symbol *.

$$Y_l^{-m}(\theta,\phi) = Y_l^m(\theta,\phi)^* \tag{9}$$

3.2 Coefficients a_{lm}

The coefficients a_{lm} are projections of $f(\theta,\phi)$ on each basis function $Y_l^m(\theta,\phi)$ over the sphere, as shown in Eq.(10). Therefore, we have two integrals computation: one for $\theta = \int_0^{\pi} d\theta$ and other for $\phi = \int_0^{2\pi} d\phi$, to cover the entire sphere surface [1].

$$a_{lm} = \int_{\theta=0}^{\pi} \int_{\phi=0}^{2\pi} f(\theta,\phi) Y_l^m(\theta,\phi) sin(\theta) d\phi d\theta \tag{10}$$

In practical terms, these coefficients provide spatial information about the structure frequencies. The higher the number of coefficients, the more detailed information that can be obtained from the 3D object. The number of coefficients is directly related to the l value, since higher values of l imply in high-frequency signals and low values of l show low-frequency information [8]. The $Y_l^m(\theta,\phi)$ (Eq.(3)) could be arranged to be a complex matrix and the matrix size is defined by the l value.

It is important to highlight that we did not find a definition regarding how much is "high" or "low" values of l in the analyzed literature. Nevertheless, we tested l values from 0 to 100 (Section 5) and we noted that l values greater than 3 could separated the 3D objects classes with 100% of precision and accuracy. In addition, we realized that the greater the value of l, the more significant the differences were between the classes, indicating the good potential of SPHARMs as a unique algorithm, useful for 3D shape analysis.

An important task on the SPHARMs computation is the coefficients a_{lm} calculation and some papers only focus on improving this. These coefficients are efficiently computed using the least squares method [9]. Eq.(11) presents the least squares method, using transposition and identity matrices, where $C \in \mathbb{R}^{NX3}$ is a Cartesian coordinate matrix composed of the N vertices of the 3D object under analysis. We have that $C = (c_0, .., c_{N-1}, c_N)^T$, where $c_i = (x_i, y_i, z_i)$ and $i \in [0, N]$.

The B term, $B \in \mathbb{N}^{DxN}$, is the matrix generated by $Y_l^m(\theta,\phi)$ (Eq.(3)), $\forall(\theta,\phi)$ of the 3D object composed of the N vertices. The D variable is the size of $Y_l^m(\theta,\phi)$, related to the definition of degree l. We have that $m \in [-l, l]$, thus $D = 2l + 1$. For example, for $l = 2$, we have $m = \{-2, -1, 0, 1, 2\}$ and $D = 5$. Consequently, we can state that the greater the value of l the more coefficients we have to represent the same in 3D object.

$$a_{lm} = (B^T B)^{-1} B^T C \tag{11}$$

3.3 Pseudo code to compute SPHARMs

One of the objectives of this paper, was to develop an algorithm to calculate the SPHARMs. Algorithm 1 analyzes each vertex in Cartesian coordinates (lines 3 to 5), and calculates the θ and ϕ (lines 6 and 7). While m is lower than l (line 9), it calculates and multiplies the values of $Y_l^m(\theta, \phi)$.

It is important to highlight that our algorithm considers the m value to apply the conjugate rule shown in Eq.(9) (line 11) and the Condon-Shortley phase shown in Eq.(8) (line 14). The computation of a_{lm}, described in Section 3.2 and Eq.(11) is presented on line 19. We created two matrices: the first one to store the results found for each pair (l, m) when $Y_l^m(\theta, \phi)$ is computed, and the second one to store the 3D object Cartesian coordinates.

ALGORITHM 1: SPHARMs calculation

Data: 3D object, value of l
Result: Matrix with the sum for each pair (l, m)

```
1  initialization;
2  while 3D object.line != null do
3      mCoord[line][x] =vertex.x;
4      mCoord[line][y] =vertex.y;
5      mCoord[line][z] =vertex.z;
6      θ = calculateTheta(vertex.x,vertex.y,vertex.z);
7      φ = calculatePhi(vertex.x,vertex.y,vertex.z);
8      m=-l;
9      while m ⩽ l do
10         if m<0 then
11             Ytemp += (-1)^m(computesY(l,|m|, θ, φ).conjugate);
12             mY[l][m]=Ytemp;
13         else
14             Ytemp += (-1)^m(computesY(l,|m|, θ, φ));
15             mY[l][m]=Ytemp;
16         end
17         m++;
18     end
       /* a_lm coefficients computing                                    */
19     coef_alm = ((mY.transpose*mY).inverse)*(mY.transpose*mCoord)
20 end
```

4 EXPERIMENT

After implementing Algorithm 1, we designed an experiment to analyze the performance of SPHARMs as shape descriptors to be used in 3D objects retrieval. Thus, the following hypotheses were enunciated:

1. SPHARMs is a good descriptor to retrieve and classify 3D objects, even with structures that have many vertices. As presented earlier, several works described the SPHARMs are widely used for classification and shape differentiation of 3D objects [53]. However, the studies do not usually fully describe the 3D objects used in the validation and it was not possible to conclude how the SPHARMs behave in different scenarios.

2. SPHARMs are computationally efficient. Several studies support this hypothesis [40, 52], but due to the complexity in some calculation steps, some studies encountered problems in the algorithm

performance [54]. Thus, in this study we want to confirm this hypothesis in the 3D medical objects retrieval.

4.1 Datasets and Material

We use two sets of 3D objects: (1) predefined synthetic cubes whose vertices and faces were well known, facilitating to check the results; and (2) 3D medical objects related to left ventricles, whose surfaces were reconstructed from MRI slices.

We performed several changes on the shape of these 3D objects aiming to validate the main SPHARMs characteristics: invariance to rotation, scale, and translation. We also validate their ability to discriminate different degrees of shape deformations.

The first group, denominated as Control Group 1 (CG1), was made up of 14 cubes, each one with 8 vertices. The following shapes changes were applied on CG1:

(1) a cube measuring 2 centimeters (cm) on each side, as shown in Fig. 4a, where the faces painted in purple and green are made to facilitate the rotation visualization;
(2) a cube built as cited in (1), but considering an increase in its scale with a factor of 0.5;
(3) three cubes with the same characteristics of (1), but rotated 60° in each axis: a cube with this change in the x axis, the other cube with change in the y axis and the last one changing the z axis, respectively, as illustrated in Fig. 4b;
(4) a cube with the same characteristics of (1), but rotated 60° in the three axes (x, y and z);
(5) nine cubes with the same characteristics of (1), where different shape changes were applied in the same vertex, increasing its original distance of 5 cm, 10 cm and 20 cm, respectively, as exemplified in Fig. 4c;

The main goal of these shape changes was to simulate shape deformations on the 3D objects, which is the main reason for using SPHARMs as a descriptor.

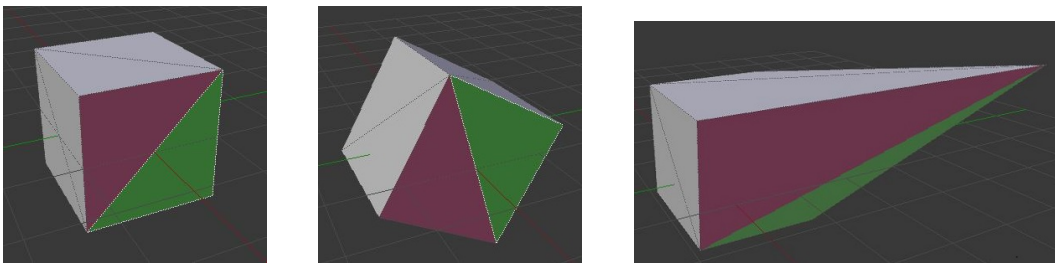

(a) Cube with dimension of 2cm in each side.

(b) Original cube rotated 60° on x axis direction.

(c) Cube with a shape change, obtained by displacing 5 cm in a vertex on y axis.

Fig. 4. Examples of synthetic objects of the Control Group 1 (CG1).

The second Control Group, named Control Group 2 (CG2) consisted of 3D surfaces of left ventricle of the human heart reconstructed from cardiac MRI slices and it was segmented considering the epicardium. (green line in Fig. 5a). Similarly to the cube, we designed this control group as follow:

(1) a left ventricle measuring approximately 4 cm of diameter. (Fig. 5b)
(2) a left ventricle built as cited in (1), but considering an increase in its scale with a factor of 0.5;
(3) a left ventricle with the same characteristics of (1), but rotated at 60° in the x axis;
(4) two left ventricles with the same characteristics of (1), where different shape changes increasing its original distance of 2 cm, and 4 cm, respectively, as illustrated in the Fig. 5c shows an example of this 2cm distance increase in the y axis;

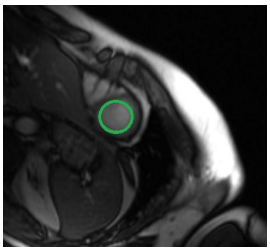

(a) MRI slice with the left ventricle segmented (green line).

(b) Left ventricle reconstructed from MRI slices.

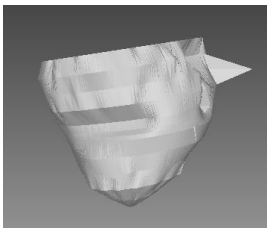

(c) Left ventricle with shape modification of 2cm in y axis.

Fig. 5. Left ventricle control group.

We used a computer with Intel i5 processor, 8GB of RAM and Windows 7 OS - 64bits. The algorithm was developed using Java JDK 1.8 in the Eclipse Helius IDE [16].

4.2 Experiment Validation

We used the similarity method proposed by Kazhdan *et al.* [25], which consists in applying a sum of Euclidean distance ($||x||_2$) for a specific degree l, as shown in Eq.(12).

$$||x||_2 = \sum_{l=0}^{\infty} \|f(\theta,\phi) - g(\theta,\phi)\|^2 \tag{12}$$

We investigated the SPHARMs performance considering two aspects: precision and efficiency. The first aspect mentioned above is related to the SPHARMs potential to differentiate shapes, as well as the capacity of SPHARMS of being invariant to scale and rotation operations. For this task we used metrics often used for image retrieval and classification: dendrograms with hierarchical clustering to visualize how the groups' hierarchy was built; silhouette, a well-known coefficient that validates the cluster consistency [38]; and Precision *vs.* Recall curve, that analyzes the fraction of relevant objects retrieved in a search. These metrics, detailed below, provide a way to compare our approach with other results from the literature about SPHARMs.

The confusion matrix indicates the algorithm performance based on the resulting cluster. It is a NxM matrix, where N is the classes and M the instances classified by the algorithm. Colors are used to better visualize and understand this matrix. In this paper, dark cells indicate high degree of one subject belonging to a class, and white cells indicate low degree of the instance belonging to that class.

The silhouette coefficient analyzes both cluster cohesion and division – as the silhouette value is closer to 1.0 the stronger the cluster groups are, values closer to zero indicate the opposite . Eqs. (13) and (14) present this coefficient computation (Sil_i). Considering an object o_i, a is the cluster that contains o_i, b is the set of all the other clusters that do not contain o_i, and db_i is the minimum of all average distances ($d_a(b)$) between o_i and the elements of each cluster of the b set.

$$db_i = min(d_a(b)) \tag{13}$$

$$Sil_i = (db_i - da_i)/max(a_i, db_i) \tag{14}$$

The accuracy, described in Eq.(15), is a metric often used in classification problems to show how well the system classifies the 3D objects. The term TP is related to *True Positive* results retrieved

during the search, TN are *True Negative* results, FP is related to the *False Positive* classifications and FN are the *False Negative* ones.

$$Accuracy = \frac{(TP + TN)}{(TP + TN + FP + FN)} \tag{15}$$

The Precision *vs.* Recall curve is a common metric used for information retrieval problems [36], in order to analyze the fraction of relevant objects retrieved in a search. Eq.(16) and Eq.(17) show, respectively, the precision and recall terms computation. The combination of these two values generates a curve. The greater the area between this curve and the x axis, the more accurate the system.

$$Precision = TP/(TP + FP) \tag{16}$$

$$Recall = TP/(TP + FN) \tag{17}$$

The second aspect analyzed concerned computational efficiency, related to: 1) to validate if our approach is feasible in real time computational systems; and 2) the impact of parameter l and number of vertices in the processing time. These aspects were chosen because Algorithm 1 uses two variables (vertices number – line 2 and l value – line 9), which can directly impact its performance, since they stipulate how many operations will be necessary to run the algorithm.

In order to accomplish the first goal, we changed the l value from 0 to 100 and observed the Algorithm behavior with different quantities of vertices in a 3D object of CG1. We applied a remeshing in the original cube and created a new set of 3D objects with 8, 56, 296, 1352 and 5048 vertices. The algorithm 1 processed each cube of CG1 changing the l value, as cited. The second objective was verified by performing an asymptotic analysis of Algorithm 1 to obtain a result from a theoretical perspective.

4.3 Experiment design

Considering the hypotheses presented in Section **??** and the aspects detailed in the previous section, we first submitted objects from the CG1 set (Section 4.1) to execute the Algorithm 1. Since the characteristics of these objects were fully known, their small number of vertices provided us the possibility to check the execution of all the steps of the Algorithm, making corrections when necessary, and finally, ensuring it worked adequately. Then, we analyzed the results of the retrieval using the metrics described in section 4.2.

After ensuring the efficiency of the SPHARMs for CG1, we repeated the process for the CG2 objects (Section 4.1), and we analyzed the results using the same metrics, as presented and discussed in the next sections.

5 RESULTS

To define the l value, we performed several tests using different values for the l parameter. We observed that values greater than 3 could properly separate the CG1, but the clusters generated had a low dissimilarity. For values greater than 50 we noticed a better cluster division, but the processing time was highly increased (Section 5.3). Thus, we found that $l = 10$ presented a good cost-benefit ratio and it was used for both Control Groups to analyze the SPHARMs precision.

We analyzed the two control groups (CG1 and CG2) separately in Section 5.1 and Section 5.2, considering the metrics described in Section 4.2, in order to evaluate the SPHARMs potential in shape differentiation as well as their invariance in relation to scale and rotation. Results of the computational efficiency are presented in Section 5.3.

5.1 Control Group 1: Cubes

Fig. 6 presents the dendrogram for CG1, which shows that there is a hierarchy between the shape modifications. It can be seen that the 3D objects which had 10 cm shape changes (Shape10X, Shape10Y, Shape10Z) from the origin were classified as more similar to the objects which had 5 cm changes (Shape5X, Shape5Y, Shape5Z) than those with 20 cm changes (Shape20X, Shape20Y, Shape20Z). This shows coherence in the functioning of SPHARMs. In addition, the original objects and the 3D objects with rotation and scaling (Original, Scaling, Rot60x, Rot60Y, Rot60Z, Rot60XYZ) were classified in the same group, indicating a total similarity among them. This indicates the SPHARMs invariance to rotation and scale.

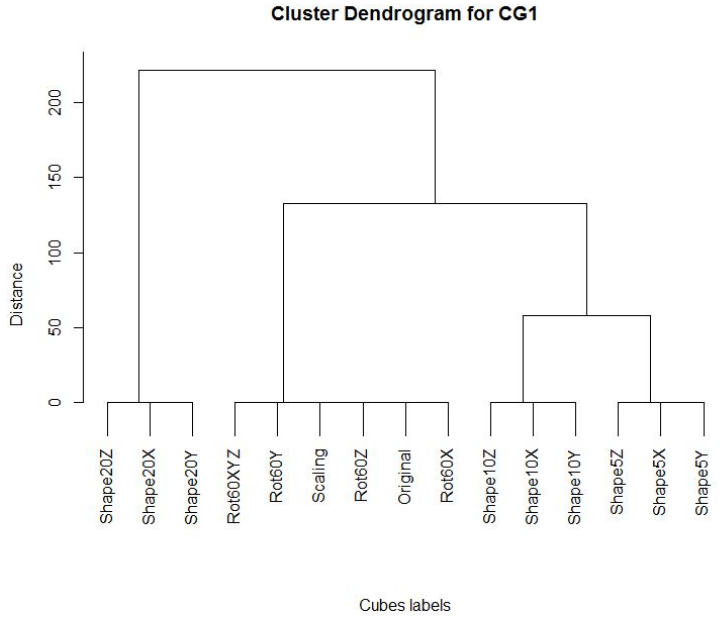

Fig. 6. Results of the CG1 (cubes) analysis using a Dendogram.

We obtained a 1.0 value of silhouette, which indicates a perfect and strong division. This value shows that, in addition to the cluster separation, the dissimilarity between each group is consistent, which leads us to believe that for more complex 3D objects, with more vertices, the SPHARMs also have the potential to present good results.

Also, we found an accuracy of 100%, indicating a complete correctness of the SPHARMs algorithm to predict the classes. This result is consistent with the results found using silhouette and dendrograms, corroborating the SPHARMs robustness in shape distinction. Considering the retrieval perspective, Fig. 7 for CG1, where darker areas indicate greater similarity among the 3D objects. These results offer clues about the algorithm capability for distinguishing objects with different shapes. It can be seen, for example, that the group which has the distance increased by 5 cm in each axis (Shape5X, Shape5Y, Shape5Z for x; y and z axes, respectively) have the same dissimilarity as the group with 10 cm distance (Shape10X, Shape10Y, Shape10Z). Moreover, this dissimilarity is smaller than the group with a 20 cm distance (Shape20X, Shape20Y, Shape20Z).

The same behavior is noted for the original cube and its respective objects where rotations and scaling operation were applied (Original, Scaling, Rot60x, Rot60Y, Rot60Z, Rot60XYZ). These latter

objects have greater similarity among themselves. Furthermore, their similarity decreases linearly in relation to the group with 5 cm, 10 cm, and 20 cm, which can be observed by the clearer cells.

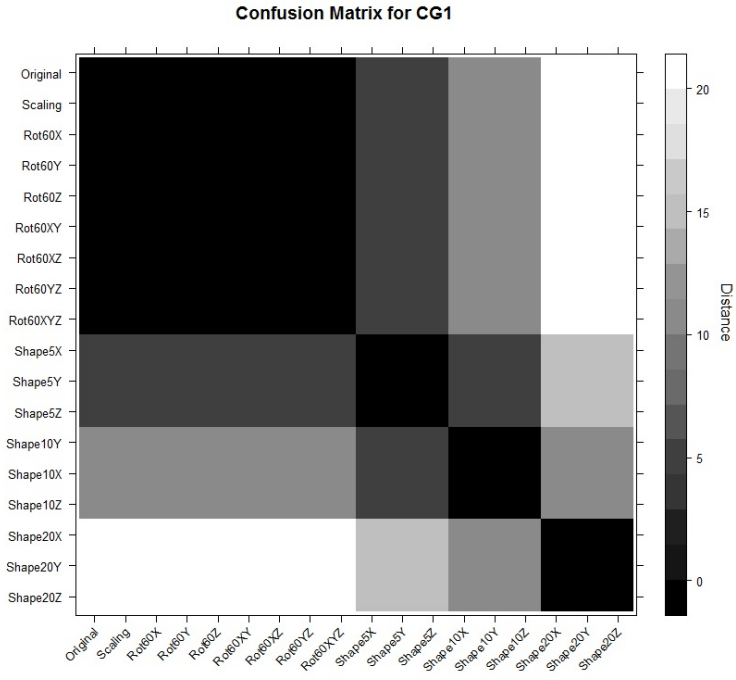

Fig. 7. Confusion matrix for CG1.

Fig. 8 presents the Precision *vs* Recall curve. This graphic was obtained computing the average precision for each recall value. Each object of the CG was given as query and we analyzed the retrieval order based on the Euclidean distance value. It is expected a distance value of zero between the original cube and the 3D objects that were submitted to rotation operations. Similarly, a zero value distance is expected among these latter objects and those submitted to scale operation or rotation operation in other axis. If this happened we could consider the result as correct. A similar behavior is expected for the subset of shape alterations: an object with displacement of 5 cm in a vertice considering a certain axis must have Euclidean distance of zero when compared to 3D object with the same displacement in the other axis.

In Figure 8 shows that the precision average for each subset (rotated, scaling, shape alteration) of CG1 maintained 100% for all Recall values. Retrieval systems commonly have a descendant curve with increasing Recall values. It is “easy" for a retrieval system to discover the first most similar objects, since in the database there are probably objects with different levels of similarity. Thus, those that present subtle differences with the object given as query are the first ones retrieved. Then, for the following queries the not so similar objects are retrieved, causing a decrease in the performance of the system. All queries retrieved the expected objects, resulting in 100% of precision.

We evaluate that the results presented here were very positive. Firstly, considering that CG1 is a set composed by 3D objects with few vertices, we could compute manually the results expected for each algorithm step and compare the results. This task ensured us that the results were correct. Secondly, These “perfect" results indicate a good potential of SPHARMs to distinguish shapes in more complex 3D structures as we will show in the next Section.

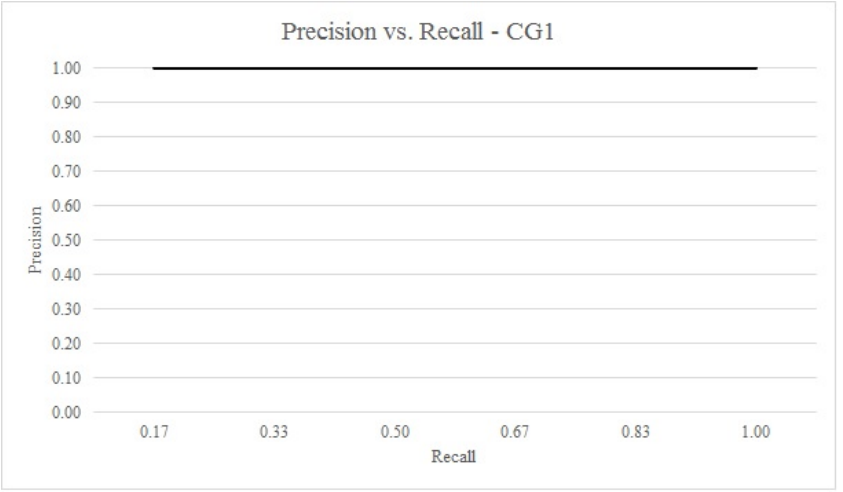

Fig. 8. Precision *vs* Recall curve for CG1.

5.2 Control Group 2: medical 3D objects

We evaluated CG2 with the same metrics used for the CG1 experiment: dendogram, silhouette coefficient, accuracy, confusion matrix and Precision *vs* Recall curve.

Fig. 9 shows the dendrogram for the CG2 results. Also in this case the SPHARMs could properly separate the 3D objects in groups. Once more, the same hierarchy related to the shape alterations can be seen. For example, the 3D objects without displacement in a vertex to increase their distance to the original 2 cm (Shape2X, Shape 2Y) are more similar to the 3D objects with 4 cm distance (Shape4X, Shape4Y) than to the original left ventricle and objects where rotation and scaling operations were applied (Original, Scaling and Rot60X).

We obtained a silhouette value of 0.63 for the entire CG2. For the 3D objects with scaling and rotation changes the silhouette was 1.0, indicating proper classification and strong differentiation among all subgroups. However, the subgroup with shape changes of 1 cm and 2 cm presented an average silhouette of 0.53. This means that although the SPHARMs have properly discriminated the different shapes, the dissimilarity between the subgroups of shapes modifications was lower compared to the CG1. This result can be justified since we have many more vertices (4900 against 12 in CG1), and also the shape modifications were subtler (1 cm and 2 cm against 5 cm and 10 cm in CG1). Despite this result, the SPHARMs algorithm still properly separated the subgroups.

We obtained 85.6% of accuracy. Also, the shape modifications subgroup impacted this value, particularly the subgroup with a 4 cm distance (Shape4X and Shape4Y). This latter group was correctly identified as having similarity with the subgroup Shape2X but not with the subgroup Shape2Y. It seems that the SPHARMs' invariance property related to rotation loses ability in 3D objects with more vertices and subtle shape modifications. In the next analysis using confusion matrix, this statement will be further explored.

Fig. 10 shows the confusion matrix for the CG2. Although the dendogram (Fig. 9) shows a proper cluster separation, the differentiation inside each subgroup is not well defined as noted in the evaluation using CG1. This is more evident for the subgroup with shape modifications. Subgroups formed by Shape4X and Shape4Y objects, for example, appear to have the same dissimilarity degree both for the subgroup with shape distance of 2 cm and for the subgroup without shape alterations.

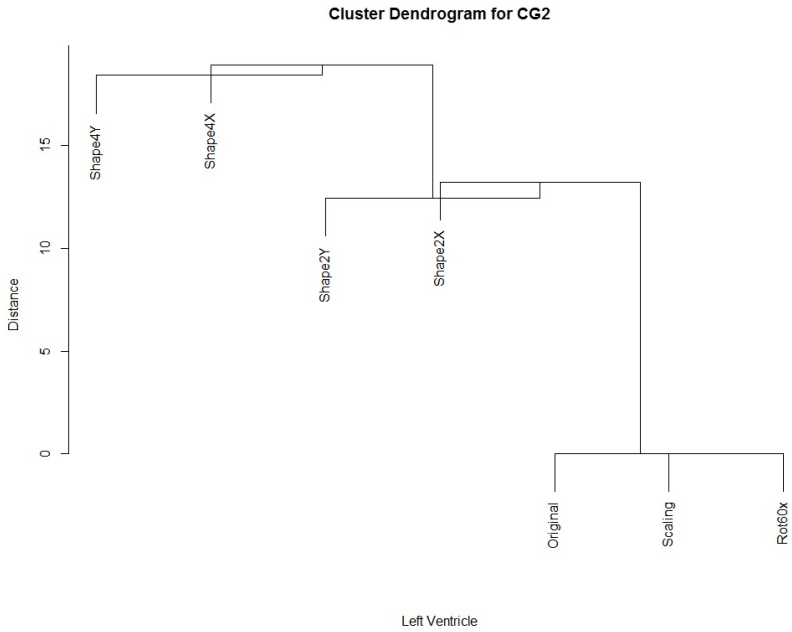

Fig. 9. Results of the left ventricle analysis using a Dendogram.

According to Fig. 10 the SPHARMs showed that the subgroup Shape4Y is more similar to 3D objects without any change than to 3D objects with shape modifications of 2 cm, which is not true.

Another highlight is that the subgroups of shape modifications are not exactly similar to their respective subgroups of objects that were submitted to rotation operation (Shape2X has a little dissimilarity degree in relation to Shape2Y, for example). This indicates a possible limitation of SPHARMs in terms of their invariance property related to rotation, which loses precision as the vertex number increases and more SPHARMs coefficients need be processed.

Fig. 11 shows the Precision *vs.* Recall curve for the CG2 3D objects. As in the evaluation using CG1, each left ventricle was given as query and we observed the retrieval order for each result. The average precision was calculated for each recall value and the final Precision *vs.* Recall curve was created. Following the tendency indicated by the other metrics, this curve also shows a decrease in precision. This specific decrease occurred due to the subgroups with shape modifications (mainly the Shape4X and Shape4Y), which first retrieved some 3D objects that belong to the original subgroup and then the Shape2X and Shape2Y objects.

5.3 Computational efficiency

We also evaluated our approach through the perspective of computational efficiency using two strategies: asymptotic analysis to validate the SPHARMs algorithm complexity and processing time evaluation considering the l value and variations for the number of vertices of the 3D objects.

Related to asymptotic analysis of Algorithm 1, we followed the directions of Cormen *et al.* [14] and considered both Legendre polynomials calculation and the SPHARMs calculation. Considering n as the size of the problem, in our case, the number of vertices, the Legendre polynomials has $O(log(n))$ complexity and SPHARMS computation has $O(n^2)$ complexity, since Algorithm 1 has a nested loop (lines 2 and 9). Thus we determined a quadratic complexity, $O(n^2)$, when $l > 1$.

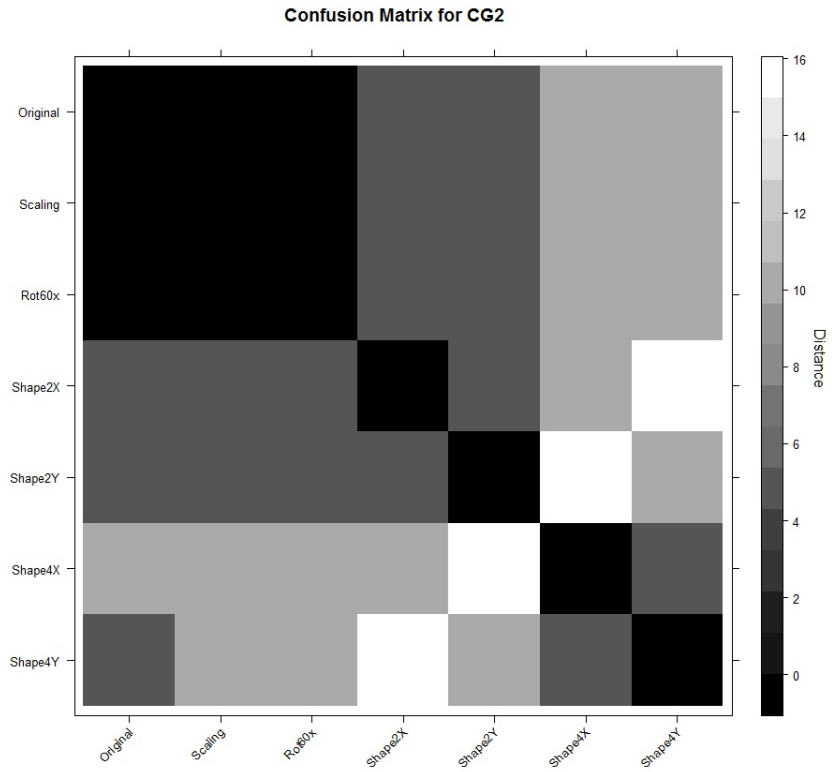

Fig. 10. Confusion matrix for CG2.

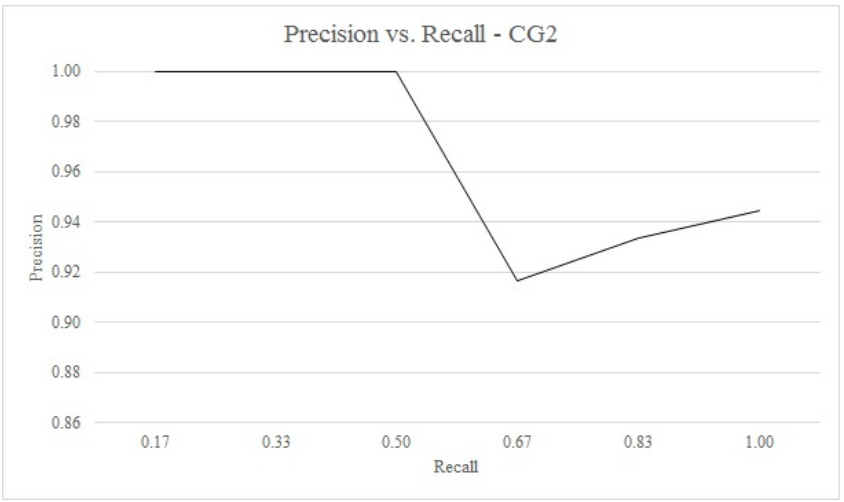

Fig. 11. Precision *vs* Recall curve for CG2.

Figs. 13(a) and 13 (b) show the time execution of Algorithm 1 accordingly to the l value variation (from 0 to 100) considering 3D objects with different number of vertices. Fig.13 (a) is related to

a 3D object of CG1 with 8 vertices and Fig.13 (b) represents the execution time of Algorithm 1 considering a 3D object with 4096 vertices of CG2.

The same behavior can be verified for both scenarios, where Algorithm 1 shows a time execution of the order of $O(n^2)$ as the l value increases, shown by the quadratic curves in both Figures.

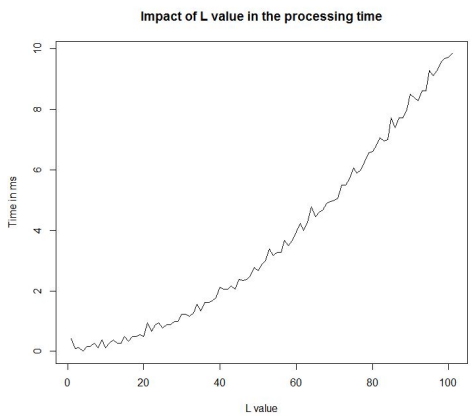

(a) Time to processing a 3D object with 8 vertices of CG1 according to l parameter variation.

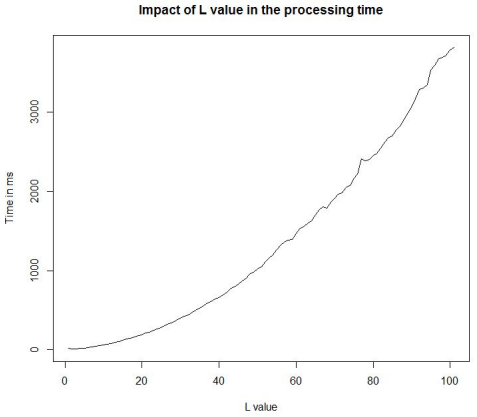

(b) Time to processing a 3D object with 4182 vertices of the CG2 according to l parameter change.

Fig. 12. Asymptotic analysis of Algorithm 1 varying l value and the number of vertices in a 3D object.

To evaluate the computational efficiency by the processing time perspective, we evaluated our approach using different l values and number of vertices for the same 3D object – the original cube of CG1 described in Section 4.1. This 3D object was remeshed, obtaining a new set of elements with different number of vertices. For each object with a different number of vertices we executed the Algorithm 1 with l varying from 0 to 100.

For the best scenario, with higher retrieval and classification precision, where $l = 10$ we achieved an average time of 1 millisecond (ms) for the object with 8 vertices and 72 ms for the object with 5048 vertices. Fig. 14 shows the time execution evolution for the size of each 3D object. It can be observed that the parameter l from Eq.(3) has the same effect on any size of 3D object and both variables: l value and number of vertices are directly related to the algorithm performance. As expected, the worst case occurred for $l = 100$ and processing of a 3D object with 5048 vertices, which took 3.99 seconds to complete the task.

This result supports our asymptotic analysis and predicting the behavior of Algorithm 1 in different scenarios. As presented in the next Section, although the complexity is $O(n^2)$, the execution time is very low compared with other algorithms that analyze information related to 3D shape of objects [6]. Besides both SPHARMs parametrization and the effect of number of vertices on the performance of the algorithm, it can be seen that independently of the number of vertices, the processing time is very similar for values of l less than 10. For example, for $l = 10$ we have 2 ms

Fig. 13. Asymptotic analysis of Algorithm 1 varying l value and the number of vertices in a 3D object: a) Time to process the 3D objects from CG1 - 8 vertices; b) Time to process the 3D objects from CG2- 4096 vertices.

for 8 vertices against 73 ms for 5048 vertices, and for $l = 100$ we obtained 26 ms for 8 vertices and 3999 ms for 5048 vertices. Thus, we had a processing time 36 times higher for $l = 10$ and 194 times higher for $l = 100$, although l only increased by 10 times.

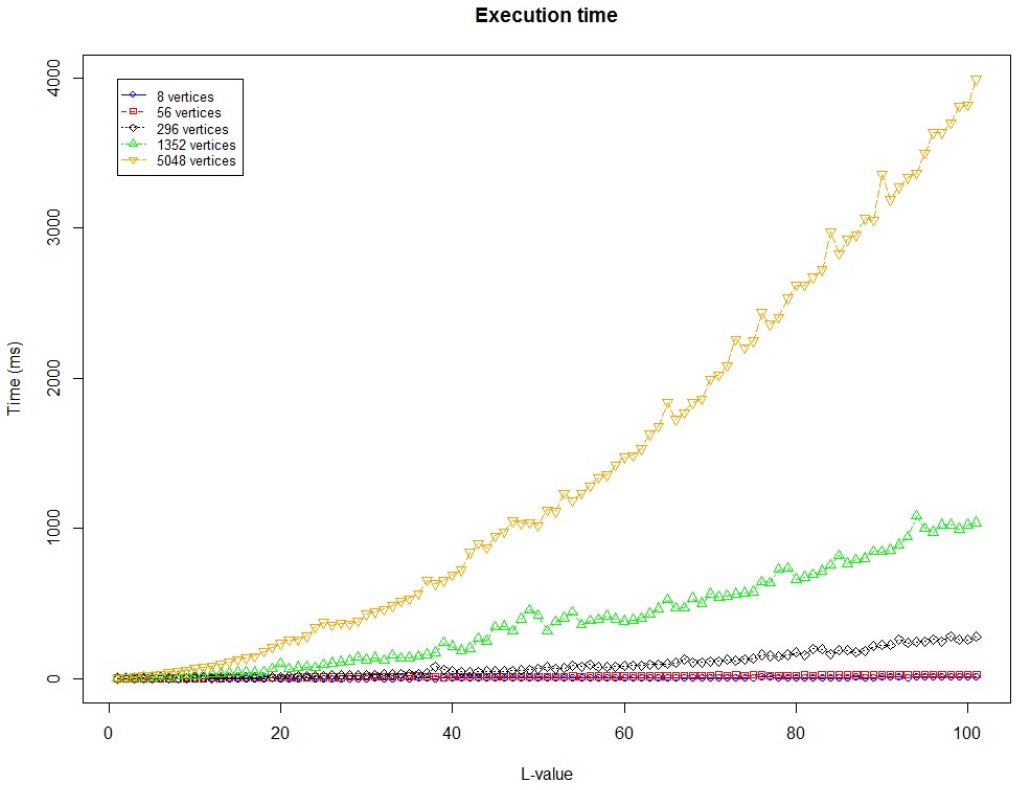

Fig. 14. Time execution of Algorithm 1 variating the l value from 0 to 100 and the number of vertices for the same 3D object.

As mentioned in Section 2, we did not find articles discussing efficiency of SPHARMs from the time execution perspective, considering 3D medical images. Only in [53], the authors commented that SPHARMs are “faster". provides a quantitative measure regarding SPHARMs performance, with a shorter execution time for 3D objects with lower number of vertices than for a higher number of vertices, but this does not necessarily mean that our approach is slow. In previous studies [6, 7] we developed other 3D shape descriptors used in very similar 3D objects, also of left ventricles from MRI images and it took 4 seconds to execute the techniques. Therefore, we got a faster result and with higher precision for complex 3D objects.

6 DISCUSSIONS

The results obtained can be seen as positive since they provide advancement in the current literature on SPHARMs. We analyzed our approach by verifying the classification and retrieval performance as well as the computational efficiency of SPHARMs.

Table 2. Average time to run the Algorithm for each 3D object

Number of vertices	Average time (milliseconds)
8	1
56	1
296	5
1352	24
5048	73

Classification and retrieval performance for CG1 were perfect, following the theoretical expectation. We achieved 100% of accuracy and average precision, a silhouette coefficient of 1.0 show how the algorithm correctly identified the different degrees of shape changes.

The results for CG2 were not perfect, but they provide better precision when compared with the study we used as reference for SPHARMs descriptor [25]. The authors applied SPHARMs in a benchmark of household 3D objects. The authors pointed out an average precision of 65-70%. Although our CG2 dataset is different from that used in [25], the 3D objects structure and shape are similar, thus achieving more than 90% of average precision. It is important to highlight that no adaptations were performed on the algorithm, following the authors' instructions; and although we expected a similar performance, we obtained a better one.

We should emphasize that although CG2 was composed of real objects re-constructed from medical images, their modifications were done manually and included artificially. However, we tried to simulate subtle changes, as in real 3D objects and that allow distinguishing objects with and without anomalies (in this case, diseases such as congestive heart failure and cardiomyopathy). The results we obtained offer evidences that SPHARMs can be used to retrieve similar objects with good performance for medical cases.

On the subject of subtle shape differentiation, in [31] the authors highlighted this SPHARMs potential. They even mentioned that for 3D objects retrieval belonging to different domains, it is interesting to use semantic techniques to improve the results. Another knowledge domain which uses the SPHARMs discrimination potential is for protein modeling, classification, and docking [24, 47]. In these works, due to the nature of the problem - small shapes, the SPHARMs obtained accuracy greater than 97%. Compared to our CGs, we obtained a better performance in CG1 but in CG2, due to the complexity of the 3D objects and number of vertices, we obtained lower performance of 3%.

Concerning computational efficiency, we found no research detailing the SPHARM algorithm complexity or information on the time to process 3D medical objects; thus, it is an important contribution to the area. Analyzing the algorithm, we obtained $O(n^2)$ complexity, which was confirmed by experimental results, showing that SPHARMs behavior was expected, according to the asymptotic analysis.

Considering other scenarios apart from the medical imaging domain, our results followed previous works: we found several papers which used SPHARMs to retrieve 3D objects [37, 47] and SPHARMs had a better performance than classic descriptors such as Light Field Descriptor (LFD). In [51] it was observed that the LFD reached about 20 seconds to retrieve each 3D object from the following databases: CCCCDatabase, National Taiwan University database (NTU) and Princeton Shape Benchmark database, adapted algorithms using SPHARMs had a processing time of less than 1 second.

Our execution time outperformed some works, such as [33, 54], which obtained an execution time of 2.4 and 4 seconds, respectively. But, since the authors did not present the number of vertices

of their 3D objects, it is not possible to conclude if our approach, without any modification on SPHARMs algorithm, impacts the result.

Our tests provide evidence that the algorithm was fast even for those 3D objects with thousands of vertices, as shown in Fig. 14. Thus, it is likely this behavior offers clues that it is possible to execute retrieval using SPHARMs in real time.

6.1 Challenges and future directions

Our research opens up several opportunities for SPHARMs research. The first one is related to SPHARM algorithm improvement, since our approach shows an $O(n^2)$ complexity, the body of research aimed at improving algorithm performance is welcome.

Secondly, as mentioned on Section 2 several of the papers reviewed did not present all details about SPHARM parametrization, except for [44], which uses $l = 15$ to describe a 3D object of a mouse). The lack of data represents limitations to reproduce the experiments. For the most part, none of the studies reviewed presented SPHARMs execution time. Therefore, our results could be used by other researchers as reference for improvements, taking advantage of our controlled experiment.

In addition, we found no research in the literature using SPHARMs to retrieve 3D medical objects, although its potential as shape descriptor is known [53]. Therefore, our paper contributes to the area by providing initial results using 3D medical objects, reconstruction of the left ventricles surface from MRI exams. The shape modifications described in Section 4.1 were made manually to preserve the reference in the controlled experiment. Thus, experiments using 3D medical objects with natural shape deformations could be performed to validate the potential of SPHARMs in shape differentiation.

Finally, SPHARMs are considered global shape descriptors. It means that the method processes the whole 3D object to extract coefficients information to be used as input of 3D modeling and classification, among other tasks. However, we noted that using the information and values we can map the coefficients extracted with the corresponding spherical coordinate, and this allows treating the SPHARMs as a local descriptor. This characteristic is very useful because: 1) complex 3D objects with hundreds of vertices can be split and decrease the time to process the information; 2) in some problems, it is desired to compare only some parts of the 3D object, which requires local descriptors; some authors have already pointed out this desirable characteristic [18, 31].

7 CONCLUSION

The potential of SPHARMs to deal with 3D objects for different tasks such as shape modeling, feature extraction and 3D objects is well cited in the literature, but the computing literature describing the “whys" and “hows" is limited. Thus, the objective of this paper was to investigate in depth the development and application of SPHARMs focused on 3D medical objects.

For achieve this goal, we developed an algorithm and tested it by conducting an experiment with two control groups: one with a synthetic 3D objects (CG1) and another with complex 3D objects, composed of left ventricles re-constructed from MRI images, using a greater number of vertices (CG2).

We achieved 100% of average precision and accuracy for CG1, and average precision greater than 90% and accuracy of 85.6% for CG2. As mentioned in Section 6 these results provide advancement in the current literature.

From the computational efficiency perspective we were able to perform an asymptotic analysis and calculate our approach complexity as $O(n^2)$. We also identified that for both scenarios, when we have a large value in l parameter and 3D objects with hundreds or thousands of vertices, the algorithm also was faster than other shape descriptors, as shown in Section **??**.

Finally, this work opens several opportunities into this knowledge area. As mentioned in Section 6, none of the literature revised presented any kind of baseline value for SPHARMS parametrization and execution time. Thus, this work can be used as reference by future researchers in planning applications of SPHARMs in tasks related to 3D objects, since we presented precision and time results using different objects in controlled experiments.

Based on the positive results found, we plan to continue using the SPHARMs to retrieve 3D medical objects of left ventricles which had shape deformation due to cardiac diseases. In a future work, we plan to apply them in daily medical routine to help physicians make more accurate diagnoses.

ACKNOWLEDGMENTS

This work was supported by the National Institute of Science and Technology Medicine Assisted by Scientific Computing, financed by Brazilian National Council of Scientific and Technological Development and Sao Paulo Research Foundation.

REFERENCES

[1] George B Arfken and Hans J Weber. 1992. *Mathematical methods for physicists* (7 ed.). Elsevier. 732 pages. https://doi.org/10.1119/1.1986189

[2] Manish Arya, William Cody, Christos Faloutsos, Joel Richardson, and Arthur Toga. 1996. A 3D medical image database management system. *Computerized Medical Imaging and Graphics* 20, 4 (1996), 269–284. https://doi.org/10.1016/S0895-6111(96)00019-5

[3] R Ayari, A Ben Abdallah, F Ghorbel, and M H Bedoui. 2017. Analysis of Regional Deformation of the Heart Left Ventricle. *{IRBM}* 38, 2 (2017), 90–97. https://doi.org/10.1016/j.irbm.2017.02.004

[4] A P Bates, Z Khalid, and R A Kennedy. 2017. Slepian Spatial-Spectral Concentration Problem on the Sphere: Analytical Formulation for Limited Colatitude #8211;Longitude Spatial Region. *IEEE Transactions on Signal Processing* 65, 6 (2017), 1527–1537. https://doi.org/10.1109/TSP.2016.2646668

[5] G Battistella, E Najdenovska, P Maeder, N Ghazaleh, A Daducci, J P Thiran, S Jacquemont, C Tuleasca, M Levivier, M Bach Cuadra, and E Fornari. 2016. Robust thalamic nuclei segmentation method based on local diffusion magnetic resonance properties. *Brain Struct Funct* (11 2016). https://doi.org/10.1007/s00429-016-1336-4

[6] Leila C C Bergamasco and Fátima L S Nunes. 2014. A New Local Feature Extraction Approach for Content-based 3D Medical Model Retrieval Using Shape Descriptor. In *Proceedings of the 29th Annual ACM Symposium on Applied Computing (SAC '14)*. ACM, New York, NY, USA, 902–907. https://doi.org/10.1145/2554850.2554873

[7] Leila C C Bergamasco and Fátima L S Nunes. 2015. Three-dimensional Content-Based Cardiac Image Retrieval using global and local descriptors. In *AMIA Annual Symposium Proceedings*. AMIA, Washinghton, USA, 1811–1820.

[8] Ch. Brechbühler, G. Gerig, and O. Kübler. 1995. Parametrization of Closed Surfaces for 3-D Shape Description. *Computer Vision and Image Understanding* 61, 2 (3 1995), 154–170. https://doi.org/10.1006/cviu.1995.1013

[9] Lindy Brett. 1988. Methods of spherical harmonic analysis. *Quarterly Journal of the Royal Astronomical Society* 29 (1988), 129.

[10] Ning Cao, Xuwei Liang, Qi Zhuang, and Jun Zhang. 2009. Approximating high angular resolution apparent diffusion coefficient profiles using spherical harmonics under BiGaussian assumption. In *SPIE Medical Imaging*, Vol. 7262. 726204–726208. https://doi.org/10.1117/12.812944

[11] Xuejiao Chen, Wenjing Li, Jing Hua, Xiaopeng Zhang, and Huiguang He. 2013. Shape manifold regression with spherical harmonics for hippocampus shape analysis. In *SPIE Medical Imaging*, Vol. 8669. 866940–866949. https://doi.org/10.1117/12.2007158

[12] F Commandeur, O Acosta, A Simon, J D Ospina Arango, J L Dillenseger, R Mathieu, P Haigron, and R de Crevoisier. 2015. Segmentation of prostate from CT scans using a combined voxel random forests classification with spherical harmonics regularization. In *SPIE Medical Imaging*, Vol. 9287. 92870F–92870F–6. https://doi.org/10.1117/12.2073489

[13] G Coppini, M Demi, P Marraccini, and A L'Abbate. 1995. 3-D heart motion from X-ray angiography. In *Computers in Cardiology 1995*. 71–74. https://doi.org/10.1109/CIC.1995.482574

[14] Thomas H Cormen, Clifford Stein, Ronald L Rivest, and Charles E Leiserson. 2001. *Introduction to Algorithms* (2nd ed.). McGraw-Hill Higher Education.

[15] Simon Eck, Stefan Wörz, Katharina Müller-Ott, Matthias Hahn, Gunnar Schotta, Karsten Rippe, and Karl Rohr. 2014. 3D shape analysis of heterochromatin foci based on a 3D spherical harmonics intensity model. In *SPIE Medical Imaging*, Vol. 9034. 90340X–90340X–6. https://doi.org/10.1117/12.2043482

[16] Eclipse. 2017. Eclipse IDE. www.eclipse.org
[17] H Edvardson and O Smedby. 2003. Compact and efficient 3D shape description through radial function approximation. *Comput Methods Programs Biomed* 72, 2 (2003), 89–97. https://doi.org/10.1016/S0169-2607(02)00126-8
[18] N Ennahnahi, M Oumsis, A Bouhouch, and M Meknassi. 2010. Fast shape description based on a set of moments defined on the unit disc and inspired by three-dimensional spherical harmonics. *IET Image Processing* 4, 2 (2010), 120–131. https://doi.org/10.1049/iet-ipr.2009.0318
[19] Robin Green. 2003. Spherical harmonic lighting: The gritty details. In *Archives of the Game Developers Conference*, Vol. 56. 4.
[20] Helmut Groemer. 1996. *Geometric applications of Fourier series and spherical harmonics*. Vol. 61. Cambridge University Press. https://doi.org/10.1017/CBO9780511530005
[21] H Huang, L Shen, R Zhang, F Makedon, and J Pearlman. 2006. A Spatio-Temporal Modeling Method for Shape Representation. In *3D Data Processing, Visualization, and Transmission, Third International Symposium on*. 1034–1040. https://doi.org/10.1109/3DPVT.2006.20
[22] H Huang, L Shen, R Zhang, F Makedon, A Saykin, and J Pearlman. 2007. A Novel Surface Registration Algorithm With Biomedical Modeling Applications. *IEEE Transactions on Information Technology in Biomedicine* 11, 4 (2007), 474–482. https://doi.org/10.1109/TITB.2007.897577
[23] H Huang, L Zhang, D Samaras, L Shen, R Zhang, F Makedon, and J Pearlman. 2006. Hemispherical Harmonic Surface Description and Applications to Medical Image Analysis. In *3D Data Processing, Visualization, and Transmission, Third International Symposium on*. 381–388. https://doi.org/10.1109/3DPVT.2006.71
[24] L Hui, L Feng, Y Jianli, and L Xiu-Ling. 2015. Side-chain flexibility in protein docking. In *2015 IEEE Conference on Computational Intelligence in Bioinformatics and Computational Biology (CIBCB)*. 1–8. https://doi.org/10.1109/CIBCB.2015.7300315
[25] Michael Kazhdan, Thomas Funkhouser, and Szymon Rusinkiewicz. 2003. Rotation invariant spherical harmonic representation of 3D shape descriptors. In *Proceedings of the 1th Eurographics/ACM SIGGRAPH symposium on Geometry processing*. Eurographics Association, Aachen, Germany, 156–164. https://doi.org/1000
[26] Michael Kazhdan, Patricio Simari, Todd Mcnutt, Binbin Wu, Robert Jacques, Ming Chuang, and Russell Taylor. 2009. A Shape Relationship Descriptor for Radiation Therapy Planning. In *Proceedings of the 12th International Conference on Medical Image Computing and Computer-Assisted Intervention: Part II (MICCAI '09)*. Springer-Verlag, Berlin, Heidelberg, 100–108. https://doi.org/10.1007/978-3-642-04271-3{_}13
[27] W B H Khelifa, A Ben Abdallah, and F Ghorbel. 2008. Three dimensional modeling of the left ventricle of the heart using spherical harmonic analysis. In *Biomedical Imaging: From Nano to Macro, 2008. ISBI 2008. 5th IEEE International Symposium on*. 1275–1278. https://doi.org/10.1109/ISBI.2008.4541236
[28] G Kiss, S Drisis, D Bielen, F Maes, J Van Cleynenbreugel, G Marchal, and P Suetens. 2006. Computer-aided detection of colonic polyps using low-dose CT acquisitions. *Acad Radiol* 13, 9 (2006), 1062–1071. https://doi.org/10.1016/j.acra.2006.05.002
[29] G Kiss, J Van Cleynenbreugel, S Drisis, D Bielen, G Marchal, and P Suetens. 2005. Computer aided detection for low-dose CT colonography. In *Med Image Comput Comput Assist Interv*. Vol. 8. 859–867. https://doi.org/10.1007/11566465{_}106
[30] T ko Tatey ama, M Okegawa, M Uetani, H Tanaka, S Kohara, X Han, S Kanasaki, S Sato, M Wakamiya, A Furukawa, H Jiang, and Y W Chen. 2012. Efficient shape representation and statistical shape modeling of the liver using spherical harmonic functions (SPHARM). In *The 6th International Conference on Soft Computing and Intelligent Systems, and The 13th International Symposium on Advanced Intelligence Systems*. 428–431. https://doi.org/10.1109/SCIS-ISIS.2012.6505370
[31] Hamid Laga, H Takahashi, and M Nakajima. 2006. Spherical Wavelet Descriptors for Content-based 3D Model Retrieval. In *Shape Modeling and Applications, 2006. SMI 2006. IEEE International Conference on*. 15. https://doi.org/10.1109/SMI.2006.39
[32] Matthew Liptrot and François Lauze. 2016. Rotationally invariant clustering of diffusion MRI data using spherical harmonics. In *SPIE Medical Imaging*, Vol. 9784. 97843C–97843C–7. https://doi.org/10.1117/12.2217090
[33] A Mademlis, P Daras, D Tzovaras, and M G Strintzis. 2009. Ellipsoidal Harmonics for 3-D Shape Description and Retrieval. *IEEE Transactions on Multimedia* 11, 8 (2009), 1422–1433. https://doi.org/10.1109/TMM.2009.2032690
[34] Martin J Mohlenkamp. 2010. *A user's guide to spherical harmonics*. Technical Report. Department of Mathematics, Ohio University.
[35] Richard J Morris, Rafael J Najmanovich, Abdullah Kahraman, and Janet M Thornton. 2005. Real spherical harmonic expansion coefficients as 3D shape descriptors for protein binding pocket and ligand comparisons. *Bioinformatics* 21, 10 (2005), 2347. https://doi.org/10.1093/bioinformatics/bti337
[36] Henning Müller, Nicolas Michoux, David Bandon, and Antoine Geissbuhler. 2004. A review of content-based image retrieval systems in medical applications—clinical benefits and future directions. *International Journal of Medical Informatics* 73, 1 (2004), 1–23. https://doi.org/10.1016/j.ijmedinf.2003.11.024

[37] Panagiotis Papadakis, Ioannis Pratikakis, Stavros Perantonis, and Theoharis Theoharis. 2007. Efficient 3D shape matching and retrieval using a concrete radialized spherical projection representation. *Pattern Recognition* 40, 9 (2007), 2437–2452. https://doi.org/10.1016/j.patcog.2006.12.026

[38] Peter J Rousseeuw. 1987. Silhouettes: A graphical aid to the interpretation and validation of cluster analysis. *J. Comput. Appl. Math.* 20 (11 1987), 53–65. https://doi.org/10.1016/0377-0427(87)90125-7

[39] Dietmar Saupe and Dejan V Vranić. 2001. 3D Model Retrieval with Spherical Harmonics and Moments. In *Pattern Recognition: 23rd DAGM Symposium Munich, Germany, September 12–14, 2001 Proceedings*, Bernd Radig and Stefan Florczyk (Eds.). Springer Berlin Heidelberg, Berlin, Heidelberg, 392–397. https://doi.org/10.1007/3-540-45404-7{_}52

[40] Volker Schönefeld. 2005. Spherical harmonics. *Computer Graphics and Multimedia Group, Technical Note. RWTH Aachen University, Germany* (2005).

[41] Peter-Pike Sloan. 2008. Stupid spherical harmonics (sh) tricks. In *Game developers conference*, Vol. 9.

[42] M Styner, G Gerig, J Lieberman, D Jones, and D Weinberger. 2003. Statistical shape analysis of neuroanatomical structures based on medial models. *Medical Image Analysis* 7, 3 (2003), 207–220. https://doi.org/10.1016/S1361-8415(02)00110-X

[43] Martin Styner, Jeffrey A Lieberman, Dimitrios Pantazis, and Guido Gerig. 2004. Boundary and medial shape analysis of the hippocampus in schizophrenia. *Medical Image Analysis* 8, 3 (2004), 197–203. https://doi.org/10.1016/j.media.2004.06.004

[44] J Su and X Zhao. 2013. Research on the describing method of 3D product shape based on Fourier operator. In *IEEE Conference Anthology*. 1–4. https://doi.org/10.1109/ANTHOLOGY.2013.6784701

[45] Katsuyuki Taguchi, Gengsheng L Zeng, and Grant T Gullberg. 2001. Cone-beam image reconstruction from equiangular sampling using spherical harmonics. In *SPIE Medical Imaging*, Vol. 4322. 867–876. https://doi.org/10.1117/12.431166

[46] Peter Guthrie Tait. 1867. *Treatise on natural philosophy*. Vol. 1. Clarendon Press. https://doi.org/10.1017/CBO9780511703935.001

[47] V Tsatsaias, P Daras, and M G Strintzis. 2007. 3D Protein Classification using Topological, Geometrical and Biological Information. In *2007 IEEE International Conference on Image Processing*, Vol. 6. VI – 537–VI – 540. https://doi.org/10.1109/ICIP.2007.4379640

[48] Gustavo Velásquez-Rodríguez, Fernando Arámbula Cosío, and Boris Escalate Ramírez. 2015. Automatic segmentation of the fetal cerebellum using spherical harmonics and gray level profiles. In *SPIE Medical Imaging*, Vol. 9681. 968114–968118. https://doi.org/10.1117/12.2207833

[49] Dejan V Vranic and Dietmar Saupe. 2004. *3D model retrieval*. Ph.D. Dissertation. University of Leipzig.

[50] D V Vranic, D Saupe, and J Richter. 2001. Tools for 3D-object retrieval: Karhunen-Loeve transform and spherical harmonics. In *2001 IEEE Fourth Workshop on Multimedia Signal Processing (Cat. No.01TH8564)*. 293–298. https://doi.org/10.1109/MMSP.2001.962749

[51] Dingwen Wang, Shilei Sun, Xi Chen, and Zhiwen Yu. 2016. A 3D shape descriptor based on spherical harmonics through evolutionary optimization. *Neurocomputing* 194 (2016), 183–191. https://doi.org/10.1016/j.neucom.2016.01.081

[52] Quan Wang, Kerstin Birod, Carlo Angioni, Sabine Grösch, Tim Geppert, Petra Schneider, Matthias Rupp, and Gisbert Schneider. 2011. Spherical harmonics coefficients for ligand-based virtual screening of cyclooxygenase inhibitors. *PloS one* 6, 7 (2011), e21554. https://doi.org/10.1371/journal.pone.0021554

[53] Faxin Yu, Zheming Lu, Hao Luo, and Pinghui Wang. 2011. *Three-dimensional model analysis and processing*. Springer Science & Business Media. 500 pages. https://doi.org/10.1007/978-3-642-12651-2

[54] C Ziyang. 2010. Retrieval of 3D Models Based on Spherical Harmonics. In *2010 International Conference on Electrical and Control Engineering*. 2991–2994. https://doi.org/10.1109/iCECE.2010.729

Received November 2018